IEEE Access
Multidisciplinary | Rapid Review | Open Access Journal

Received January 12, 2017, accepted February 21, 2017, date of publication March 1, 2017, date of current version June 7, 2017.

Digital Object Identifier 10.1109/ACCESS.2017.2675378

Low-Profile Design of Broadband High Gain Circularly Polarized Fabry-Perot Resonator Antenna and its Array with Linearly Polarized Feed

ZHEN-GUO LIU[1,2], (Member, IEEE), AND WEI-BING LU[1,2]
[1]State Key Lab. of Millimeter Waves, School of Information Science and Engineering, Southeast University, Nanjing 210096, China
[2]School of Information Science and Engineering, Southeast University, Nanjing 210096, China

Corresponding author: Zhen-Guo Liu (liuzhenguo@seu.edu.cn) and Wei-Bing Lu (wblu@seu.edu.cn)

This work was supported by the National Natural Science Foundation of China under Grant 61671147 and Grant 61671150.

ABSTRACT A novel low profile broadband circularly polarized Fabry-Perot resonator antenna (CP-FPRA) with a linearly polarized feed is proposed. The goal of this antenna is to generate circular polarization with high gain level in broad bandwidth, while maintaining low profile and simple feed configuration. The proposed antenna consists of a primary radiator aligned along 45° with linear polarization, a partially reflective surface, and a nonstandard artificial magnetic conductor acting as a reflective ground plane. Its profile can be reduced to a quarter of a wavelength. Furthermore, an array antenna of 2×2 arrangement using CP-FPRA as element with a compact sequential rotation feeding scheme is also proposed and fabricated to enhance the gain and to improve the axial ratio (AR) bandwidth. The array was optimized to minimize grating lobes and reduce the sidelobe level, even though the element spacing was about two wavelengths. Reasonable agreement between the simulated and measured results is observed. The measured common bandwidth of $|S_{11}| \leq -10$ dB, gain-drop $\leq$3 dB, and AR $\leq$3 dB is about 7.4%.

INDEX TERMS Fabry-Perot resonator antenna, circularly polarized, low-profile, partial reflective surface, artificial magnetic conductor.

I. INTRODUCTION

In satellite and radar systems, where both high gain and circular-polarized (CP) antennas are required, CP-FPRA can be a good candidate due to its characteristics of compact structure and high gain performance. FPRA generally consists of a simple primary radiator embedding inside a cavity formed by placing a PRS half a wavelength above a conducting ground plane. With attractive features of high-gain and simple feeding FPRA have aroused significant interest recently [1]–[19]. From the viewpoint of a primary radiator there are two approaches can be used to realize CP-FPRA (1) a PRS is placed directly above a CP feeding antenna [20]–[22], and (2) a PRS is arranged directly above an linearly polarized (LP) feed which typically tilts by 45° with respect to the axes [23]–[30]. In approach (1), a PRS is used to form an FP cavity only. And the circularly polarized feeding network is generally required [20]–[22], which will increase the complexity of the whole structure. In approach (2), in fact, the PRS must perform two functions simultaneously: one is to form the FP cavity integrating with the ground plate, and the other is to act as a polarizing transforming structure to convert the LP radiation of the feed into CP radiation, which can avoid using complex CP feed networks. Recently some interesting works have been done on the CP-FPRA based on approach (2). In [24], the CP-FPRA with a printed PRS consisting of rectangular patches array excited by an LP dipole was firstly presented. By adjusting the aspect ratio of the rectangular patch element, the LP radiation produced by the feed can be transformed into CP radiation. In [25], a CP-FPRA with a quarter wavelength corrugation acting as a ground plane was introduced. A CP-FPRA with a double-sided PRS was also presented in [27] and [28]. In [29], a completely metallic FPRA with stacked FP cavities, covered by an LP to CP converting layer, was proposed. A summary of comparison between previously reported designs of CP-FPRA related to approach (1) and

TABLE 1. Comparison between reported CP-FPRA.

Ref.	App	Prof.	Config. of PRS and Ground	Com BW(%)
[20]	1	$1.4\lambda_0$	3 layers dielec. Slabs + Gr.	1.3 (Mea)
[21]	1	$0.5\lambda_0$	Ring FSS printed on single dielec. Slab + Gr.	10.4 (Simu)
[22]	1	$0.2\lambda_0$	FSS printed on single dielec. Slab + Squa. type AMC	1.5 (Mea)
[23]	2	$0.67\lambda_0$	3 layers metal Grid FSSs + Gr.	2 (Mea)
[24]	2	$0.5\lambda_0$	Rect. FSS printed on single dielec. Sheet + Gr.	7.7 (Simu)
[25]	2	$0.75\lambda_0$	Single Metal Cross slot FSS + Corrugated Gr.	1.9 (Mea)
[26]	2	$0.5\lambda_0$	Patch+truncated corners FSS printed on dielec. Slab + Gr.	4.1 (Mea)
[27]	2	$0.5\lambda_0$	Strip FSSs printed on two dielec. Sheets + Gr.	6.8 (Simu)
[28]	2	$0.45\lambda_0$	2 layers FSSs printed on single dielec. Slab + HIS	2 (Mea)
[29]	2	$0.95\lambda_0$	2 layers metal Grid FSSs + Corrugated Gr.	3 (Mea)

approach (2) is presented in Table 1, in which "Com BW" means the common bandwidth of $|S_{11}| \leq -10$dB, gain-drop $\leq$ 3dB, and AR $\leq$ 3dB. The profile of CP-FPRA that mentioned above are always of a half wavelength or even more. It results this kind of antenna is not suitable for being used in some low-profile or conformal situations.

To minimize the overall CP-FPRA profile, while processing broadband CP characteristic and keeping the compact feeding structure, this paper presents a novel broadband CP-FPRA, which comprises an LP microstrip patch aligned along 45°, a PRS formed by cross-slot array, and a non-standard AMC surface. The profile of the whole structure is only a quarter of a wavelength. The proposed antenna generates a CP beam with a moderate gain. Furthermore, in order to enhance the gain and improve the AR bandwidth, a CP-FPRA array of 2×2 elements with sequential rotation feeding approach is implemented as well. This paper is organized as follows. In Section II, the analysis model and design method are described in detail. In Section III, the design of a low profile CP-FPRA fed by an LP microstrip patch is presented. Simulation results are presented to verify the feasibility and validity of design model. The prototype antenna fabrication and measured results are discussed in Section IV. In Section V, the design method of an array composed of 2×2 CP-FPRA elements with sequential rotation feeding scheme and measured results are proposed. Finally, in Section VI the conclusions are drawn.

II. MODELING AND DESIGN METHOD

A. PRS STRUCTURE AND CP GENERATION CONDITION

Fig.1 shows the configuration of the proposed CP-FPRA. It consists of a microstrip patch aligned along 45° with linear polarization, a metallic PRS formed by periodical cross-slot

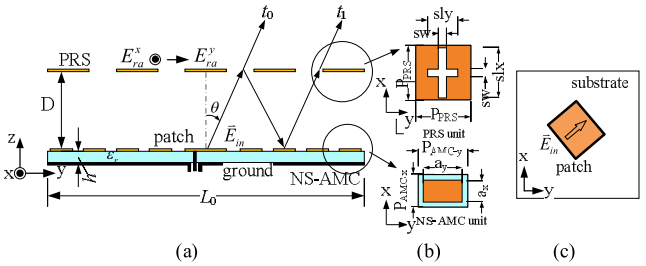

FIGURE 1. The configuration of proposed CP-FPRA (a) side view, (b) PRS unit, and NS-AMC unit, (c) Microstrip Patch.

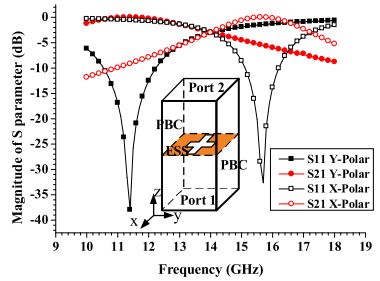

FIGURE 2. The frequency response of the S parameters of the PRS unit cell.(a) Magnitude. (b) Phase.

array and a nonstandard AMC acting as reflective ground plane. A 45° linearly polarized excitation $\vec{E}_{in}$ can be decomposed into two orthogonal in-phase components $\vec{E}^{x}_{in}$ and $\vec{E}^{x}_{in}$ of equal amplitude. At the same time, the radiated or transmitted wave $\vec{E}_{ra}$ from the upper surface of the PRS can be expressed as two orthogonal components $\vec{E}^{x}_{ra}$ and $\vec{E}^{y}_{ra}$. When CP wave operation is required, the condition of these two orthogonal components with the same magnitude and a 90° phase difference need to be satisfied. It also means that we can make use of the characteristics of the transmission of the PRS to simply analyze the CP generation condition. Its transmission characteristics corresponding to x- and y-polarization incident can be derived by unit cell (as shown in Fig.1b and Fig.2a) simulation based on periodic boundary condition (PBC). For simplicity only normal incidence is considered and the incident electric field is polarized along the x and y direction, respectively. Then the model in which the transmission characteristics of s^{x}_{21} and s^{y}_{21} corresponding

to x and y polarization incident can be obtained is simulated by HFSS. By tuning the two perpendicular slots with different resonant length such that, one of the slots (x-directed slot) resonates below f_0, the center frequency, whereas the other (y-directed slot) resonates higher than f_0, then the required CP generation condition can be fulfilled. The magnitude and phase frequency response of the transmission coefficients for different polarizations are shown in Fig. 2. It demonstrates that, at the operating frequency $f_0 = 14$ GHz, an identical magnitude of s_{21}^x and s_{21}^y with 90° phase difference between them is achieved simultaneously. Fig.2b also shows the reflection coefficient characteristics for the two polarizations. It is noted that a phase difference of 270° (or −90°) between the reflection coefficients s_{11}^x and s_{11}^y of the PRS in operating frequency is obtained automatically.

An interesting phenomenon is worth noting that for a CP-FPRA fed by LP primary source, as mentioned above, according to the phase difference between s_{11}^x and s_{11}^y provided by PRS structure, there are two completely different types of PRS structures. One is a purely metallic PRS such as a cross-slot type structure [25], which can provide a ±90° phase difference between s_{11}^x and s_{11}^y automatically. It can be explained in detail in Appendix I. The other one is a dielectric-metallic type PRS such as a rectangular microstrip patch printed on the bottom surface of a dielectric sheet [24], [26] or two sets of periodic metallic strips printed on the opposite sides of the single layer substrate [27] or printed on two layer dielectric substrates [28], which provides an equal phase between s_{11}^x and s_{11}^y. Thus the different relationships between s_{11}^x and s_{11}^y caused by PRS will result in different FP structure particular in height of cavity to satisfy the corresponding resonance condition. In addition, due to its single layer purely metallic PRS structure, the cost of the former is relative low compared with the latter dielectric-metallic PRS structure.

B. NONSTANDARD AMC STRUCTURE AND CAVITY RESONANCE CONDITION

In order to realize the CP-FPRA, except for CP generation condition, the FP resonance condition also need to be satisfied. In this paper, an AMC structure consisting of a rectangular patch array printed on a substrate backed with a ground plane is proposed to set up resonance condition. Full-wave simulations on the unit cells (as shown in Fig.1c and Fig.3) were carried out to estimate the reflection characteristics of the AMC sheets. The FP resonance condition can be expressed by

$$\begin{cases} -4\pi D/\lambda_0 + \varphi_{PRS}^x + \varphi_{AMC}^x = 2n\pi \\ -4\pi D/\lambda_0 + \varphi_{PRS}^y + \varphi_{AMC}^y = 2n\pi \end{cases} \tag{1}$$

where D is the height of the cavity, λ_0 is the free space wavelength of the centre frequency, n is an integer, $\varphi_{PRS}^x \varphi_{PRS}^y$ (also the phase of s_{11}^x and s_{11}^y mentioned above) and φ_{AMC}^x, φ_{AMC}^y are the phases of the reflection coefficients for the PRS and AMC in x- and y-polarizations, respectively. In order to keep the same cavity height at resonance for both polarizations, a 90° phase difference between φ_{AMC}^x and φ_{AMC}^y is used to compensate the phase difference caused by metallic PRS, which is achieved by tuning the aspect ratio of the rectangular patch in the unit cell of the AMC. On the other hand, in order to reduce the profile, the absolute values of φ_{AMC}^x and φ_{AMC}^y need to be considered carefully. For a cavity with height of a quarter wavelength, the first term in formula (1) is equal to $-\pi$. Accounting for the phase values of s_{11}^x and s_{11}^y at the operating frequency, and letting $n = 0$ in formula (1), then φ_{AMC}^x and φ_{AMC}^y are obtained as 45° and −45° respectively. Compared with a traditional AMC whose reflection phase is close to zero at the operating frequency, we called this type of AMC a nonstandard AMC.

III. SIMUATION AND CALCULATION OF MODEL

A CP-FPRA based on the concept presented above is shown in Fig.1. The simulated S_{11} of proposed CP-FPRA for different D dimensions is shown in Fig. 4a. It can be seen that there are two types of independent resonance mechanisms. One is contributed by the source microstrip patch. Its resonance determines by patch size. And the other one corresponds to the cavity resonance which mainly determined by cavity height. The bandwidth of the impedance matching can be improved by adjusting these two types of resonances. It is illustrated that the resonant frequency of cavity mode will decrease as the cavity height D increases from 5.4 mm to 5.8 mm. The frequency response of the gain for LHCP

$$\begin{aligned} T_{FP}^{x/y} &= f(\theta,\varphi)\sum_{n=0}^{\infty} t_n^{x/y} = f(\theta,\varphi)\sum_{n=0}^{\infty} (r_{AMC}^{x/y} r_{PRS}^{x/y})^n t^{x/y} e^{-jkn2D\cos\theta} \\ &= t^{x/y}/(1 - r_{AMC}^{x/y} r_{PRS}^{x/y} e^{-jk2D\cos\theta}) f(\theta,\varphi) \\ &= (1 + r_{PRS}^{x/y})/(1 - r_{AMC}^{x/y} r_{PRS}^{x/y} e^{-jk2D\cos\theta}) f(\theta,\varphi) \end{aligned} \tag{2}$$

$$\left|T_{FP}^{x/y}\right|^2 = \frac{|f(\theta,\varphi)|^2 \times (1 - \left|r_{FSS}^{x/y}\right|^2)}{1 - 2\left|r_{AMC}^{x/y}\right|\left|r_{PRS}^{x/y}\right|\cos(\varphi_{AMC}^{x/y} + \varphi_{PRS}^{x/y} - k2D\cos\theta) + \left|r_{AMC}^{x/y}\right|^2\left|r_{PRS}^{x/y}\right|^2} \tag{3}$$

$$AR = \sqrt{g + \sqrt{g^2 - 4\sin^2\varphi}}/\sqrt{g - \sqrt{g^2 - 4\sin^2\varphi}} \tag{4}$$

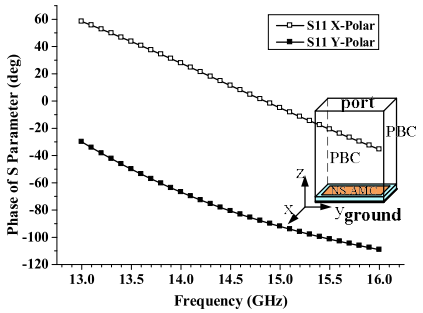

FIGURE 3. The frequency response of the reflection coefficient phase of the AMC unit cell for x- and y- polarization.

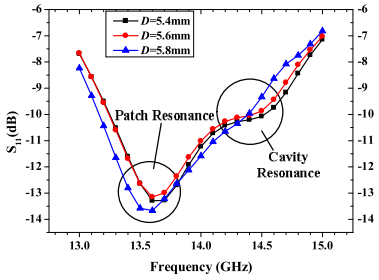

(a)

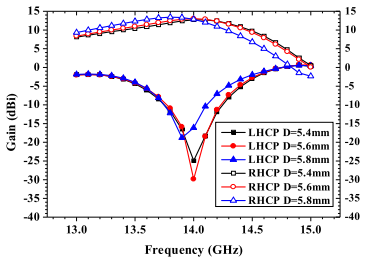

(b)

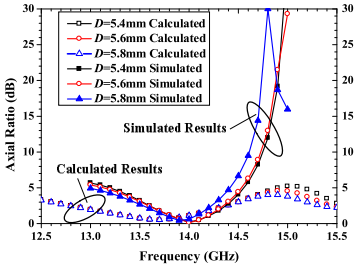

(c)

FIGURE 4. Simulated results of the proposed CP-FPRA for different cavity heights D, (a) Reflective coefficient, (b) gain response, (c) axial ratio response.

and RHCP with different D is also shown in Fig. 4b. The frequency of peak gain shifts down as the cavity height D increases. The antenna dimensions for the optimized design are given in Table 2.

Based on the ray viewpoint, the total transmitted wave power outside the resonator cavity with respect to angle and frequency, $|T_{FP}(\theta, f)|^2$, can be calculated by a superposition of all partially transmitted fields, as shown in Fig. 1, which is expressed as [1], where $t^{x/y}$ is the direct transmitted field,

TABLE 2. Final dimensions for the CP- FPRA.

Antenna lateral size	L_0=49mm
Cavity height	D=5.4mm
Metallic PRS Parameters	t=1mm, P_{PRS}=13.9mm, slx=13.6mm, sly=10.2mm, sw=3.0mm
NS-AMC Parameters	$P_{AMC\text{-}x}$=3.7mm, $P_{AMC\text{-}y}$=5.5mm, a_x=3.0mm, a_y=4.5mm
Radiator Patch	L_p = 7.4 mm, W_p = 6.5mm
Substrate	h=1.575mm, ε_r =2.2

$r_{AMC}^{x/y}$ is the complex reflection coefficient of the AMC with phase $\varphi_{AMC}^{x/y}$, $r_{PRS}^{x/y}$ is the reflection coefficient of PRS with phase $\varphi_{PRS}^{x/y}$ corresponding to x- and y polarization respectively. Here k is the wavenumber in free space, and $f(\theta, \varphi)$ denotes the radiation pattern of primary radiator tilted at 45° situation, which is derived in detail in Appendix II by simple coordinate transform method. Then the axial ratio can be calculated using the following simple relation [30].

where $g = \rho + 1/\rho$, $\rho = \left|T_{FP}^x\right| / \left|T_{FP}^y\right|$, and $\varphi = \angle T_{FP}^x - \angle T_{FP}^y$.

Fig.4c shows the simulated results (from HFSS) and the calculated results (from formula (4)) of the AR frequency response in the broadside direction. The good agreement of simulated results and calculated results in the frequency bandwidth region from 13.8GHz to 14.4GHz indicates that the method and principle of taking use of the complex reflection coefficients of PRS and AMC to control and generate the circular polarization is correct and feasible. At the same time, we also observed that the calculated results of AR yield a wider bandwidth compared with the simulated results. It may be caused by: 1) the size of PRS in the calculation procedure according to formulas (2)-(4), as shown at the bottom of the previous page, is infinite, which is different from the actually simulated model; 2) the reflection coefficient of the primary feed is not considered in the calculation, which is different from the simulation; 3) the radiation pattern of the primary feed in calculation is approximated, while the simulation procedure makes no such assumption.

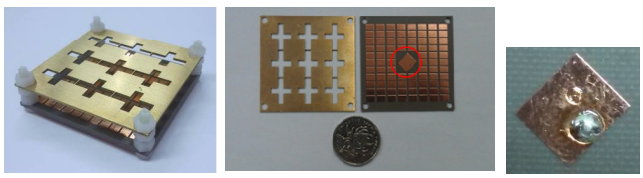

(a) (b) (c)

FIGURE 5. Photograph of the proposed CP-FPRA, (a) solid view (b) PRS and NS-AMC (c) exciting Patch.

IV. EXPERIMENT AND MERSUREMENT

Fig.5 shows the prototype of proposed antenna. The simulated and measured S_{11} is shown in Fig. 6a. There is a good agreement between simulation and measurement except for a frequency downward shift. The measurements of axial ratio, gain and radiation patterns are carried out in an

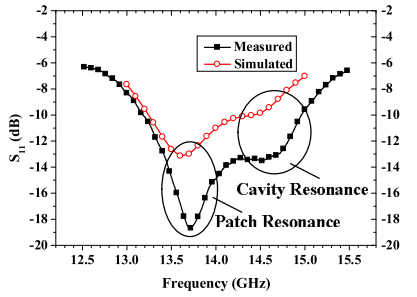

(a)

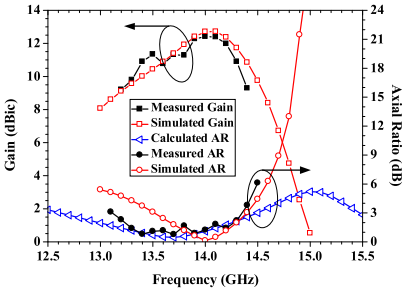

(b)

FIGURE 6. Simulated and measured results of the proposed CP-FPRA, (a) Reflective coefficient, (b) axial ratio and gain responses.

anechoic chamber. The measured 3-dB AR bandwidth is from 13.3 GHz to 14.2 GHz as shown in Fig.6b, which is narrower than that of simulated results. The gain of the circularly polarized antenna was obtained using the correction factor of polarization as follows [31]:

$$G = G_0 + 3 + 20\log(1/2(1 + 10^{-AR/20}))\text{dBi} \qquad (5)$$

where G_0 is the measured gain by horn antennas. Fig. 6b also shows the simulated and measured gain of the proposed antenna. Compared with simulated results, the measured 3-dB gain bandwidth is from 13.3 GHz to 14.4 GHz which is a little wider than the simulated one. The maximum measured gain is about 12.4 dBi at 13.9 GHz, which has a 0.3 dB drop from the simulated result. Thus, the common bandwidth for the -10 dB impedance match, 3-dB AR, and 3-dB gain drop, is from 13.3 GHz to 13.8 GHz. Fig.7 shows the normalized results of simulated and measured radiation pattern of the CP-FPRA at center frequency. The difference between the simulated and measured results shown in Fig.6 and Fig.7 may be caused by inexact and inconsistent distance between the PRS and substrate of prototype during the course of mechanical mounting.

V. ANTENNA ARRAY

In order to enhance the gain and improve the bandwidth of FPRA, a possible method is to employ an antenna array instead of a single antenna as the primary source [3], [31]. As shown in Fig. 8, a CP-FPRA array, using the CP-FPRA itself to act as sub-array, with a sequential rotation feeding approach [32] is proposed. The four sequentially rotated

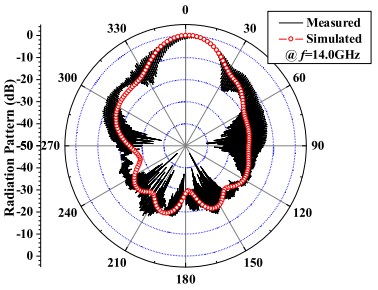

FIGURE 7. Normalized measured and simulated radiation pattern of the proposed CP-FPRA at f=14.0 GHz.

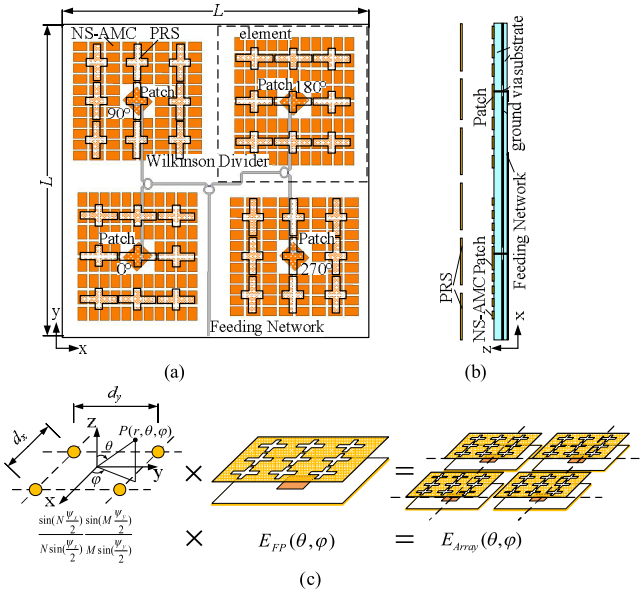

FIGURE 8. The geometry of proposed CP-FPRA array with a sequential rotation feeding scheme, (a) top view, (b) side view, (c) principle of radiation pattern excited by CP-FPRA array.

antenna elements are fed with a phase distribution of 0°, 90°, 180° and 270° by employing a microstrip feeding network composed of three Wilkinson dividers and different length transmission lines corresponding to a phase delay of 90° with respect to the adjacent element. The microstrip feeding network is printed on a dielectric sheet with a relative permittivity of 2.2 and a thickness of 0.254 mm. In contrast to previous studies on FPRA excited by conventional planar arrays [2] where the space between elements is about half a wavelength, adopted technique in here results in the distance between two adjacent elements is much larger than the typical value of standard arrays, which derives the larger effective radiating area of each element. It will perform reduction of mutual coupling between elements, but will potentially suffer from high level of grating lobe. According to array theory, the radiation pattern of the antenna array can be calculated as the product of the array factor with the radiation pattern of the single element, as shown in Fig.8c, where $\psi_x = kd_x \sin\theta\cos\varphi$, and $\psi_y = kd_y \sin\theta\sin\varphi$, $d_{x/y}$ is the distance between two elements and M/N is the number of unit cells along the x/y directions, respectively. Here, M and N are

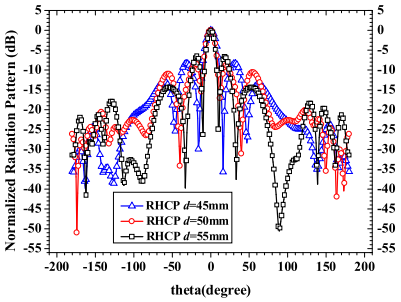

FIGURE 9. Simulated normalized radiation pattern of proposed CP-FPRA array for different element spacing d.

equal to 2. $E_{FP}(\theta, \varphi)$ is the radiation pattern of the single CP-FPRA element, which can be calculated by formula (3). In this case, the distance between two adjacent elements is about $2\lambda_0$. For a general uniform antenna array, the element of which having a low directivity, the grating lobe condition is determined mainly by array factor. When spacing of inter-element is about $2\lambda_0$, it will lead to the appearance of grating lobes. The first grating lobe is relative to $\lambda_0/d_{x/y}$. However, for the CP-FPRA array proposed here, each element (i.e., each CP-FPRA) has a relatively high directivity and the number of element is small, so the radiation pattern of the element that mainly defines the grating lobe condition. For example, if let $d_{x/y}$ be equal to $2\lambda_0$, then the grating lobe θ_{gl} is located in $\pm 30°$ according to the formula in [33], which corresponds to a level of -11 dB in the radiation pattern of the CP-FPRA element. Hence, the grating lobe will not be a serious problem.

In addition, the angle of the first side lobe of the antenna array is given by [33]

$$\theta_{sl} = \pm \arcsin(3\lambda/2Nd_{x/y}) \tag{6}$$

If let $d_{x/y}$ be equal to $2\lambda_0$ and $N = 2$, then first side lobe θ_{sl} is situated in $\pm 22°$, which corresponds to the level of -7.5 dB in the radiation pattern of the CP-FPRA element. Thus the side lobe is a factor that needs to be considered carefully. The spacing of inter-element is a crucial parameter that affects the gain and the side lobe level of the antenna array. Fig.9 shows the simulated normalized radiation pattern for different d ($d = d_x = d_y$). As d changes from 55 mm to 45 mm, the side lobe location is increased from $\pm 18°$ to $\pm 31°$, and its corresponding level is also decreased from -6.5 dB to -9.5 dB, which coincides well with calculation by formula (6). The final optimum determination of the spacing $d = 52.5$ mm is done by simulation. Fig.10 shows a photograph of the fabricated CP-FPRA array with the sequential rotation feeding scheme. Fig.11a shows the simulated and measured S_{11} frequency response of CP-FPRA array. It is observed that there is a frequency shift in the resonance, which may be caused by fabrication error and alignment error in the height of the cavity. This results in an impedance bandwidth ($|S_{11}| \leq -10$ dB) that is narrower than the simulated one. Fig.11b plots the simulated and measured

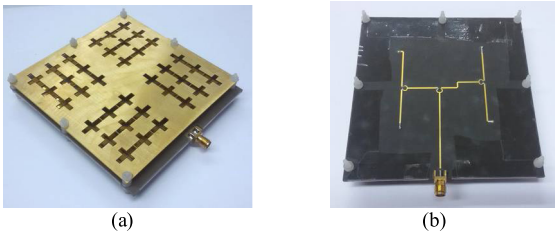

FIGURE 10. Photograph of proposed CP-FPRA array with sequential rotation feeding scheme, (a) solid view, (b) bottom view.

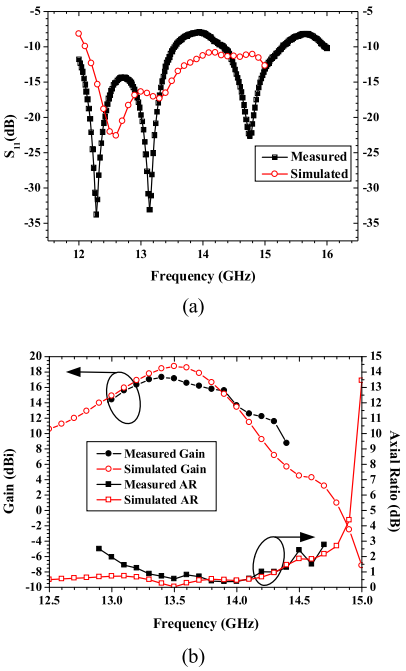

FIGURE 11. Simulated and measured results of the proposed CP-FPRA array (a) Reflective coefficient, (b) axial ratio and gain responses.

AR and RHCP gain against the frequency, which almost have the similar trends. Due to the sequential rotation feeding scheme, the simulated 3dB AR bandwidth are 2.8GHz (12.0-14.8GHz), which is much wider than that of single CP-FPRA element. The measured 3-dB AR bandwidth is from 12.9 GHz to 14.7 GHz, which is narrower than that of simulated results. The measured 3-dB gain bandwidth is from 12.95 GHz to 13.95 GHz with peak gain of 17.2 dBi at 13.4 GHz, which is less than the simulated result of 18.6 dBi at 13.5 GHz. At final, measured common frequency bandwidth of CP-FPRA array is about 7.4% from 12.95GHz to 13.95GHz. Fig.12 shows the normalized results of measured radiation patterns of the CP-FPRA array at various frequencies. It is demonstrated that the side lobe locations agree well with those calculated from formula (6) and the side lobe levels are general about -9 dB, which is slightly higher than the simulated one. Beam tilting is also observed in the measured radiation pattern. It may be caused by unsymmetrical ground plane, which is for the convenient of mounting the coaxial cable connector to excite the feeding network as shown in Fig.10.

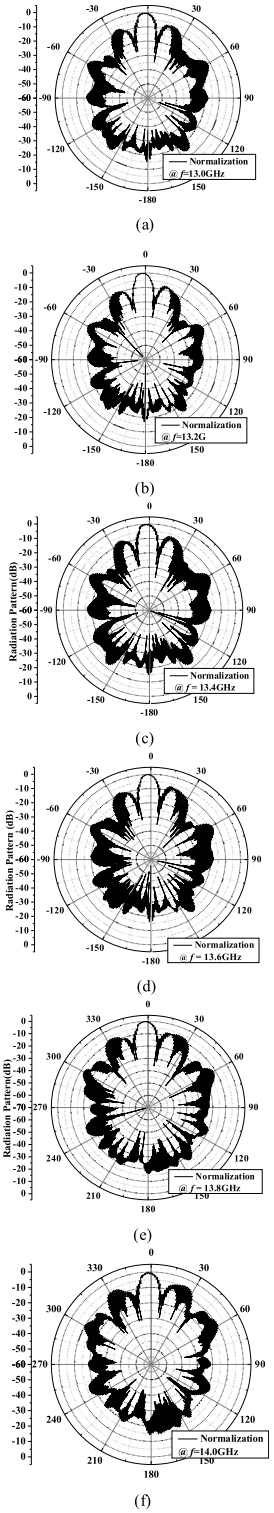

FIGURE 12. Normalized measured radiation patterns for the proposed CP-FPRA array, at (a) f = 13.0 GHz, (b) f = 13.2 GHz, (c) f = 13.4 GHz, (d) f = 13.6GHz, (e) f = 13.8GHz, (f) f = 14.0GHz.

VI. CONCLUSION

This paper presented a broadband low-profile circularly-polarized Fabry-Perot resonator antenna (CP-FPRA) fed by an LP microstrip patch aligned along 45°, which consists of a partially reflective surface formed by cross-slot array, and a nonstandard AMC acting as reflective ground plane. Taking use of PRS and AMC structure, the profile of antenna can be reduced to a quarter wavelength. A prototype antenna with a common frequency bandwidth of 6.4% for $|S_{11}| \leq -10$dB, and gain-drop $\leq$ 3 dB, and AR $\leq$ 3 dB, with a size of $49\times49\times5.4$ mm^3 was validated by simulation and measurement. At same time, a concept of using the CP-FPRA itself to act as sub-array to increase the gain and AR bandwidth is also presented. A CP-FPRA array of 2×2 elements with a compact sequential rotation feeding scheme was simulated and fabricated. Its measured common frequency bandwidth is about 7.4% from 12.95GHz to 13.95GHz. In addition, a simple design and calculation method for this type antenna is also introduced.

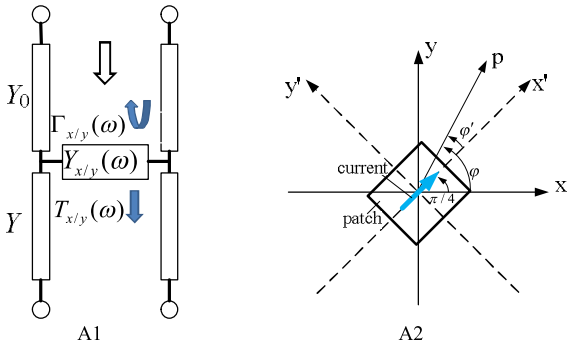

FIGURE 13. (A1) Transmission model of purely lossless PRS, (A2) Configuration of current tilts by 45° with respect to the axes.

APPENDIX I

In this section, we will find the phase relation between reflection and transmission coefficient of the purely metallic PRS in normal incidence. Assuming a purely metallic lossless PRS can be modelled by a frequency dependent admittance $Y_{x/y}(\omega) = jB_{x/y}(\omega)$ as shown in Fig.13(A1), where x/y presents the polarization of incident plane wave. Then the reflection and transmission coefficient can be expressed as:

$$\Gamma_{x/y}(\omega) = -\frac{Y_{x/y}(\omega)}{2Y_0 + Y_{x/y}(\omega)}, \quad T_{x/y}(\omega) = \frac{2Y_0}{2Y_0 + Y_{x/y}(\omega)} \tag{A-1}$$

where Y_0 is characteristic admittance of free space. The phase value of the reflection and transmission coefficients can be written as

$$\angle\Gamma_{x/y}(\omega) = -\pi/2 - \tan^{-1}(\frac{B_{x/y}(\omega)}{2Y_0}),$$
$$\angle T_{x/y}(\omega) = -\tan^{-1}(\frac{B_{x/y}(\omega)}{2Y_0}) \tag{A-2}$$

In order to realize circular polarization, that means the phase condition (A-3) must be obtained.

$$\angle T_x(\omega_0) - \angle T_y(\omega_0) = -\tan^{-1}(\frac{B_x(\omega_0)}{2Y_0}) + \tan^{-1}(\frac{B_y(\omega_0)}{2Y_0}) = \pi/2 \tag{A-3}$$

Then we can write the phase difference between the reflection coefficient of both polarizations as

$$\begin{aligned}\psi(\omega_0) &= \angle\Gamma_x(\omega_0) - \angle\Gamma_y(\omega_0)\\ &= -\pi/2 - \tan^{-1}\left(\frac{B_x(\omega_0)}{2Y_0}\right) - \left(-\pi/2 - \tan^{-1}\left(\frac{B_y(\omega_0)}{2Y_0}\right)\right)\\ &= -\tan^{-1}\left(\frac{B_x(\omega_0)}{2Y_0}\right) + \tan^{-1}\left(\frac{B_y(\omega_0)}{2Y_0}\right) = \pi/2 \quad \text{(A-4)}\end{aligned}$$

So for a purely lossless PRS structure, if the circular polarization generation condition is satisfied, the phase difference of ±90° between the reflection coefficient for both orthogonal polarization is also realized simultaneously.

APPENDIX II

In this section, we derive the radiation pattern of microstrip patch when aligning along 45° situation by transformation of coordinates method. Fig. 13(A2) shows the configuration of current tilts by 45° with respect to the axes. P is observed field point.

According to the Fig. 13(A2), $\varphi' = \varphi - \pi/4, \theta' = \theta$. When the excited current is dipole like, the far field is expressed as

$$E_{\theta'} = E_0 \cos\theta' \cos\varphi', E_{\varphi'} = E_0(-\sin\varphi') \quad \text{(A-5)}$$

$$\begin{aligned}|f(\theta,\varphi)|^2 &= |E_\theta|^2 + \left|E_\varphi\right|^2 = |E_0|^2\left(\cos^2\theta'\cos^2\varphi' + \sin^2\varphi'\right)\\ &= |E_0|^2\left[\cos^2\theta\cos^2(\varphi - \pi/4) + \sin^2(\varphi - \pi/4)\right]\\ &= |E_0|^2\left[\frac{1}{2}(1 + \cos^2\theta) - \sin^2\theta\cos\varphi\sin\varphi\right]\end{aligned} \quad \text{(A-6)}$$

where $E_0 = -j\omega\mu_0 e^{jkr}/4\pi r$. If the current on the patch is assuming to $\cos(\pi x'/L)$ ((1,0) mode), where L is the length in x' direction, then far field can be written as

$$|f(\theta,\varphi)|^2 = (|E_\theta|^2 + \left|E_\varphi\right|^2)\left|\tilde{J}_{sx}^{(1,0)}(k_x,k_y)\right|^2 \quad \text{(A-7)}$$

where $\tilde{J}_{sx}^{(1,0)}(k_x,k_y)$ is the Fourier transform of patch current, it can be expressed as:

$$\tilde{J}_{sx}^{(1,0)}(k_x,k_y) = \left(\frac{\pi WL}{2}\right)\sin c\left(k_y\frac{W}{2}\right)\left[\frac{\cos(k_x\frac{L}{2})}{(\frac{\pi}{2})^2 - (k_x\frac{L}{2})^2}\right] \quad \text{(A-8)}$$

$$\begin{aligned}k_x &= k_0\sin\theta\cos(\varphi - \pi/4),\\ k_y &= k_0\sin\theta\sin(\varphi - \pi/4)\end{aligned} \quad \text{(A-9)}$$

where W is the width of the patch. According to the formula (A-5)-(A-9), the directivity of FPRA with feed aligning along 45° can be calculated simply.

ACKNOWLEDGMENT

The authors would like to acknowledge Prof. David. R. Jackson for his helpful work on this paper.

REFERENCES

[1] G. V. Trentini, "Partially reflecting sheet array," *IRE Trans. Antennas Propagat.*, vol. 4, pp. 666–671, Sep. 1956.

[2] A. R. Weily, K. P. Esselle, T. S. Bird, and B. C. Sanders, "Dual resonator 1-D EBG antenna with slot array feed for improved radiation bandwidth," *Proc. Inst. Elect. Microw. Antennas Propag.*, vol. 1, no. 1, pp. 198–203, Feb. 2007.

[3] R. Gardelli, M. Albani, and F. Capolino, "Array thinning by using antennas in a Fabry-Perot cavity for gain enhancement," *IEEE Trans. Antennas Propag.*, vol. 54, no. 7, pp. 1979–1990, Jul. 2006.

[4] T. H. Vu, K. Mahdjoubi, and A. C. Tarot, "Bandwidth enlargement of planar EBG antennas," in *Proc. Antenna Propag. Conf. Loughborough*, Loughborough, U.K., 2007, pp. 125–128.

[5] Z. G. Liu, W. X. Zhang, and D. L. Fu, "Broadband Fabry–Perot resonator printed antennas using FSS superstrate with dissimilar size," *Microw. Opt. Technol. Lett.*, vol. 50, no. 6, pp. 1623–1627, 2008.

[6] Z. G. Liu, "Quasi-periodic structure application in Fabry–Perot resonator printed antenna," in *Proc. Asia–Pasific Microw. Conf.*, HongKong, Dec. 2008, pp. 1–4.

[7] Y. Ge, K. P. Esselle, and T. S. Bird, "The use of simple thin partially reflective surfaces with positive reflection phase gradients to design wideband, low-profile EBG resonator antennas," *IEEE Trans. Antennas Propag.*, vol. 60, no. 2, pp. 743–750, Feb. 2012.

[8] A. P. Feresidis and J. C. Vardaxoglou, "High gain planar antenna using optimised partially reflective surfaces," *IEE Proc. Microw. Antennas Propag.*, vol. 148, no. 6, pp. 345–350, 2001.

[9] A. Pirhadi, M. Hakkak, F. Keshmiri, and R. K. Baee, "Design of compact dual band high directive electromagnetic bandgap (EBG) resonator antenna using artificial magnetic conductor," *IEEE Trans. Antennas Propag.*, vol. 55, no. 6, pp. 1682–1690, Jun. 2007.

[10] M. U. Afzal, K. P. Esselle, and B. A. Zeb, "Dielectric phase-correcting structures for electromagnetic band gap resonator antennas," *IEEE Trans. Antennas Propag.*, vol. 63, no. 8, pp. 3390–3399, Sep. 2015.

[11] M. U. Afzal and K. P. Esselle, "A low-profile printed planar phase correcting surface to improve directive radiation characteristics of electromagnetic band gap resonator antennas," *IEEE Trans. Antennas Propag.*, vol. 64, no. 2, pp. 276–280, Feb. 2016.

[12] D. R. Jackson and A. A. Oliner, "A leaky-wave analysis of the high-gain printed antenna configuration," *IEEE Trans. Antennas Propag.*, vol. 36, no. 7, pp. 905–910, Jul. 1988.

[13] T. Zhao, D. R. Jackson, J. T. Williams, H. Y. Yang, and A. Oliner, "2D periodic lecky wave antenna part1: Metal patch design," *IEEE Trans. Antennas Propag.*, vol. 53, no. 11, pp. 3505–3514, Nov. 2005.

[14] T. Zhao, D. R. Jackson, and J. T. Williams, "2D periodic lecky wave antenna part 2: Slot design," *IEEE Trans. Antennas Propag.*, vol. 53, no. 11, pp. 3515–3524, Nov. 2005.

[15] M. Thevenot, C. Cheype, A. Reineix, and B. Jecko, "Directive photonic-bandgap antennas," *IEEE Trans. Microw. Theory Techn.*, vol. 47, no. 11, pp. 2115–2122, Nov. 1999.

[16] C. Cheype, C. Serier, M. Thevenot, T. Monediere, A. Reineix, and B. Jecko, "An electromagnetic bandgap resonator antenna," *IEEE Trans. Antennas Propag.*, vol. 50, no. 9, pp. 1285–1290, Sep. 2002.

[17] Y. J. Lee, J. Yeo, R. Mittra, and W. S. Park, "Application of electromagnetic bandgap (EBG) superstrates with controllable defects for a class of patch antennas as spatial angular filters," *IEEE Trans. Antennas Propag.*, vol. 53, no. 1, pp. 224–235, Jan. 2005.

[18] Z. G. Liu, "Fabry–Perot resonator antenna," *J. Infr. Millim. Terahertz Waves*, vol. 31, no. 4, pp. 391–403, 2010.

[19] Z. G. Liu, R. Qiang, and Z. X. Cao, "A novel broadband Fabry–Perot resonator antenna with gradient index metamaterial superstrate," in *Proc. IEEE Int. Symp. Antennas Propag.*, Toronto, ON, Canada, Jul. 2010, pp. 1–4.

[20] A. R. Weily, K. P. Esselle, T. S. Bird, and B. C. Sanders, "High gain circularly polarized 1-D EBG resonator antenna," *Electron. Lett.*, vol. 42, no. 18, pp. 1012–1013, Apr. 2006.

[21] Z. G. Liu and Z. X. Cao, "Circularly polarized Fabry–Perot resonator antenna," in *Proc. Int. Conf. Microw. Technol. Comput. Elecromagn.*, Beijing, China, Nov. 2009, pp. 18–21.

[22] G. Zhao, Y. C. Jiao, F. Zhang, and X. Yang, "High gain circularly polarized antenna using sub-wavelength resonant cavity," *J. Electromagn. Waves Appl.*, vol. 24, pp. 33–40, Aug. 2010.

[23] M. Diblanc, E. Rodes, E. Arnaud, M. Thevenot, T. Monediere, and B. Jecko, "Circularly polarized metallic EBG antenna," *IEEE Microw. Wireless Compon. Lett.*, vol. 15, no. 10, pp. 638–640, Oct. 2005.

[24] Z. G. Liu, "Fabry–Perot resonator antenna with polarization transform," in *Proc. IEEE Int. Symp. Antennas Propag.*, Toronto, ON, Canada, Jul. 2010, pp. 1–4.

[25] S. A. Muhammad, R. Sauleau, and H. Legay, "Self-generation of circular polarization using compact Fabry–Perot cavity antennas," *IEEE Antenna Wireless Propag. Lett.*, vol. 10, pp. 907–910, Sep. 2011.
[26] J. Ju, D. Kim, W. Lee, and J. Choi, "Design method of a circularly polarized antenna using Fabry-Perot cavity structure," *ETRI J.*, vol. 33, no. 2, pp. 163–168, 2011.
[27] S. C. Chiu and S. Y. Chen, "High-gain circularly polarized resonant cavity antenna using FSS superstrate," in *Proc. IEEE Int. Symp. Antennas Propag.*, Spokane, Washington, USA, Jul. 2011, pp. 2242–2245.
[28] R. Orr, G. Goussetis, and V. Fusco, "Design method for circularly polarized Fabry–Perot cavity antennas," *IEEE Trans. Antennas Propag.*, vol. 62, no. 1, pp. 19–26, Jan. 2014.
[29] S. A. Muhammad, R. Sauleau, and H. Legay, "Self-polarizing Fabry–Perot antennas based on polarization twisting element," *IEEE Trans. Antennas Propag.*, vol. 61, no. 3, pp. 1032–1040, Apr. 2013.
[30] Z. G. Liu, Y. X. Guo, and Z. X. Cao, "Compact low-profile circularly polarized Fabry–Perot resonator antenna fed by linearly microstrip patch," *IEEE Antenna Wireless Propag. Lett.*, vol. 15, pp. 524–527, Sep. 2016.
[31] C. R. Liu, Y. X. Guo, X. Y. Bao, and S. Q. Xiao, "60-GHz LTCC integrated circularly polarized helical antenna array," *IEEE Trans. Antennas Propag.*, vol. 60, no. 3, pp. 1329–1335, Sep. 2012.
[32] J. Huang, "A technique for an array to generate circular polarization using linearly polarized elements," *IEEE Trans. Antennas Propag.*, vol. 34, no. 9, pp. 1113–1124, Sep. 1986.
[33] C. A. Balanis, *Antenna Theory Analysis and Design*, 3rd ed. Hoboken, NJ, USA: Wiely, 2005, ch. 6.

ZHEN-GUO LIU was born in Jiangsu, China, 1973. He received the B.S. degree from Soochow University, Suzhou, China, in 1996, and the M.S. and Ph.D. degrees from Southeast University, Nanjing, China, in 2002 and in 2013, respectively. From 2005 to 2006, he was a Visiting Scholar with the Department of Electronic and Telcommunication, Politecnico di Torino, Italy. From 2011 to 2012, he was a Research Staff Member with the Department of Electrical and Computer Engineering, National University of Singapore, Singapore. From 2014 to 2015, he was a Post-Doctoral Visitor with the Department of Electrical and Computer, University of Houston. Since 2002, he has been with the School of Information Science and Engineering, Southeast University, where he is currently an Associate Professor. His current research interests involve antenna theory and application, wearable functional devices, and metamaterial antenna.

WEI BING LU was born in Jiangsu, China, in 1977. He received the B.S. and M.S. degrees from Northeast Normal University, Changchun, China, in 1999 and 2002, respectively, and the Ph.D. degree from Southeast University, Nanjing, China. He joined the State Key Laboratory of Millimeter Waves, Southeast University, in 2005, and then was promoted to an Associate Professor and a Professor in 2006 and 2008, respectively. He is currently the Vice Dean of the School of Information Science and Technology, Southeast University. His research interests include computational electromagnetic and fast algorithms, electromagnetic compatibility, antenna. He has authored or co-authored over 90 journal and conference publications. He was interested in graphene-based devices, such as absorbers, transmission lines, and antennas.

Dr. Lu received the Young Scholarship from the HuaYing Education and Culture Foundation, in 2007, the Excellent PhD Dissertation of Jiangsu Province, in 2006, the New Century Excellent Scholar Award from the Chinese Ministry of Education, in 2008, and the Award of Six Talent Peaks Project in Jiangsu Province, in 2016. In 2013, he visited the ECE Department with the University of California at San Diego, San Diego, as a Visiting Scholar, supported by HuaYing Education and Culture Foundation.